Monthly Notices of the ROYAL ASTRONOMICAL SOCIETY

MNRAS **507,** 2930–2936 (2021) https://doi.org/10.1093/mnras/stab2269
Advance Access publication 2021 August 9

Radiative association of atomic and ionic nitrogen

Zhi Qin [1,2] Tianrui Bai[1,3] and Linhua Liu[1,3,4]★

[1]*Optics & Thermal Radiation Research Center, Institute of Frontier and Interdisciplinary Science, Shandong University, Qingdao, Shandong 266237, China*
[2]*School of Information Science and Engineering, Shandong University, Qingdao 266237, China*
[3]*School of Energy and Power Engineering, Shandong University, Jinan 250061, China*
[4]*School of Energy Science and Engineering, Harbin Institute of Technology, Harbin 150001, China*

Accepted 2021 July 30. Received 2021 July 1; in original form 2021 May 24

ABSTRACT

Radiative association for the formation of molecular nitrogen cation N_2^+ during the collision of an $N(^4S_u)$ atom and an $N^+(^3P_g)$ ion is investigated. The corresponding cross-sections and rate coefficients are computed by the quantum mechanical method based on *ab initio* potential energy curves and transition dipole moments, which are obtained by the internally contracted multireference configuration interaction method with the Davidson correction and aug-cc-pCV5Z-DK basis set. A number of low-lying doublet, quartet, and sextet states correlating to the $N(^4S_u) + N^+(^3P_g)$ dissociation limit are considered. Hence, we investigate a number of dipole-allowed transitions and determine their contributions to the radiative association. The results show that transitions originating in the $f^4\Pi_u$, $D^2\Pi_g$, $B^2\Sigma_u^+$, $1^4\Sigma_g^+$, and $1^6\Sigma_u^+$states are the main contributors for the radiative association process. The calculated rate coefficients are valid for temperatures from 100 to 10 000 K and fitted to the analytical function suitable for astrochemical reaction applications.

Key words: astrochemistry – molecular data – molecular processes.

1 INTRODUCTION

The importance of molecular nitrogen cation N_2^+ has long been recognized in atmospheric phenomena including aurorae and airglows (Jones 1971; McCormack 1971; Paschmann, Haaland & Treumann 2012; Chamberlain 1961). The N_2^+ Meinel bands were first identified in the aurora at wavelengths longer than 9000 Å (Jones 1971; Lofthus & Krupenie 1977). Emissions from the first negative band for N_2^+ were first seen in the twilight (Slipher 1933) and were subsequently observed in the airglow during the day (Zipf Jr & Fastie 1964; Wallace & McElroy 1966; Feldman 1973). The spectra of N_2^+ also occurred in comet tails (Swings 1943; Herzberg 1971). Recent observations of the spectra from the C/2016 R2 (Pan-STARRs) and C/2015 V2 (Johnson) comets showed very strong emission bands from the N_2^+ ion (Venkataramani & Ganesh 2018; Raghuram, Bhardwaj & Hutsemékers 2021). Moreover, in the nitrogen atmospheres of the icy bodies in the solar system, particularly of Titan, Triton, and Pluto, there are a rich chemical composition of the ionosphere containing N, N^+, N_2^+, and other N-bearing molecules and ions (Cravens et al. 2006; Dutuit et al. 2013; Scherf et al. 2020; Erkaev et al. 2021).

N_2^+ is an important molecule in astrochemistry, as it is one of the species participating in the chemistry of Earth's and Titan's atmospheres (Cravens et al. 2006; Dutuit et al. 2013; Falcinelli et al. 2016; Scherf et al. 2020) and in physico-chemical modelling of the ion-density distribution in the inner coma of comet C/2016 R2 (Pan-STARRs) (Venkataramani & Ganesh 2018; Raghuram et al. 2021). Hence, it is necessary to securely characterize the abundance of N_2^+ as the subsequent reaction of generating other species needs available N_2^+. In this work, we consider the formation of N_2^+ by the radiative association process in collisions of a nitrogen atom and a nitrogen cation

$$N\left(^4S_u\right) + N^+\left(^3P_g\right) \rightarrow N_2^+ + h\nu. \quad (1)$$

The process in equation (1) is feasible in astrochemical environments due to the abundance of nitrogen and reaction conditions, such as Titan's ionosphere (Dutuit et al. 2013)

The theory and methodology of radiative association processes for diatomic molecules and ions have been well established and been summarized by a recent work reviewed by Nyman, Gustafsson & Antipov (2015). Computational methods for obtaining radiative association cross-sections include the perturbation theory, optical potential approach, semi-empirical method, classical approach, and Breit–Wigner theory. The perturbation theory and optical potential method are quantum mechanically based. The semi-empirical method is derived from the optical potential method. These methods have been used for dealing with many diatomic molecules and ions, such as HeH^+, PS, SiO, TiO, C_2, CO, CO^+, MgO, CS, CH^+, etc. (Gianturco & Giorgi 1997; Stancil & Dalgarno 1997; Singh et al. 1999; Stancil et al. 2000; Barinovs & van Hemert 2006; Andreazza & Marinho 2007; Andreazza, Vichietti & Marinho 2009; Andreazza et al. 2012; Andreazza, de Almeida & Borin 2016; Cairnie et al. 2017; Andreazza, de Almeida & Vichietti 2018; Forrey et al. 2018; Babb, Smyth & McLaughlin 2019a, 2019b; Gustafsson & Forrey 2019; Zámečníková, Soldán & Gustafsson 2019; de Almeida, Andreazza & Borin 2020; Forrey et al. 2020; Zámečníková, Gustafsson & Nyman 2020; Bai, Qin & Liu 2021).

In typical astrophysical applications with abundant nitrogen, the photoionization reaction $N_2 + h\nu \rightarrow N_2^+ + e$ (Zipf Jr & Fastie

★ E-mail: liulinhua@sdu.edu.cn

1964, Sharp 1974) and the charge transfer reaction $O^+ + N_2 \rightarrow N_2^+ + O$ (Broadfoot & Hunten 1966) and $N_2^+ + NO \rightarrow NO^+ + N_2$ (Fehsenfeld, Dunkin & Ferguson 1970) generally outpace reaction (1). Even so, there is a previous semi-empirical calculation of the rate coefficients of reaction (1) at temperatures from 300 to 14 700 K (Andreazza & Singh 1997) which has been included in the UMIST data base for astrochemical applications (McElroy et al. 2013). Andreazza & Singh (1997) did not include other transition processes except for the $A^2\Pi_u \rightarrow X^2\Sigma_g^+$ and $B^2\Sigma_u^+ \rightarrow X^2\Sigma_g^+$ transitions because no available experimental data were available at that time. Based on the quantum mechanical theory, we revisit reaction (1) including ten possible transition processes and compute their cross-sections, which are then used to calculate the rate coefficients of N_2^+. The results show that the dominant transition processes for the formation of N_2^+ by reaction (1) include not only the $B^2\Sigma_u^+ \rightarrow X^2\Sigma_g^+$ transition, but also the $f^4\Pi_u \rightarrow b^4\Pi_g$, $D^2\Pi_g \rightarrow A^2\Pi_u$, $1^4\Sigma_g^+ \rightarrow a^4\Sigma_u^+$, and $1^6\Sigma_u^+ \rightarrow 1^6\Sigma_g^+$ transitions. Hence, the computed rate coefficients for the formation of N_2^+ by reaction (1) are larger than those given by Andreazza & Singh (1997). Moreover, we presented the rate coefficients below 300 K down to 100 K.

This work is organized as follows. The theory and methods for computing the electronic structures, radiative association cross-sections, and rate coefficients of N_2^+ are presented in Section 2. Results and discussions for the potential energy curves (PECs), transition dipole moments (TDMs), cross-sections, and rate coefficients are given in Section 3. In Section 4, conclusion is drawn.

2 THEORY AND METHODS

2.1 PECs and TDMs

To describe the electronic states of a diatomic system, the electronic states which correlate with the dissociation channels are needed to be identified. Here, we considered the electronic states of N_2^+ which dissociate into the first channel N (^4S_u) + N^+ (^3P_g). According to Wigner–Witmer rules (Herzberg 1950), twelve electronic states, including the $X^2\Sigma_g^+$, $A^2\Pi_u$, $B^2\Sigma_u^+$, $D^2\Pi_g$, $1^4\Sigma_g^+$, $f^4\Pi_u$, $a^4\Sigma_u^+$, $b^4\Pi_g$, $1^6\Sigma_g^+$, $1^6\Pi_u$, $1^6\Sigma_u^+$, and $1^6\Pi_g$ states, were identified to dissociate into the first channel.

The PECs and TDMs were calculated with the MOLPRO 2015 quantum chemistry package (Werner et al. 2015, 2020). MOLPRO cannot take advantage of the full symmetry of non-Abelian groups. Hence, an Abelian subgroup needs to be adopted for molecules with degenerate symmetry. That is, for N_2^+ with $D_{\infty h}$ symmetry, it will be substituted by D_{2h} symmetry. The D_{2h} point group holds (A_g, B_{3g}, B_{2g}, B_{1g}, B_{1u}, B_{2u}, B_{3u}, and A_u) irreducible representations and the corresponding relationships with $D_{\infty h}$ point group are as follows: $\sigma_g \rightarrow (a_g, b_{1g})$, $\sigma_u \rightarrow (a_u, b_{1u})$, $\pi_g \rightarrow (b_{2g}, b_{3g})$, and $\pi_u \rightarrow (b_{2u}, b_{3u})$. In our calculations, the molecular orbitals (MOs) and energies of the ground state were computed by the Hartree–Fock (HF) self-consistent field method. Then, the state-averaged complete active space self-consistent field calculations (Knowles & Werner 1985; Werner & Knowles 1985) were carried out for the twelve electronic states to generate multiconfiguration wavefunctions by using the HF MOs as the starting orbitals. Finally, the internally contracted multireference configuration interaction including Davidson correction (icMRCI + Q) calculations (Knowles & Werner 1988; Werner & Knowles 1988; Knowles & Werner 1992; Shamasundar, Knizia & Werner 2011) were performed to consider the dynamic correlation and size-consistency error. The aug-cc-pCV5Z-DK Gaussian basis set was selected to describe the nitrogen atom with the consideration of core–valence correlation and scalar relativistic effects. The core–valence correlation effect was considered by putting all electrons of N_2^+ into the active space, which includes thirteen MOs, i.e. $4a_g$, $2b_{3u}$, $2b_{2u}$, $3b_{1u}$, $1b_{2g}$, and $1b_{3g}$ MOs. The scalar relativistic effect is taken into account by the third-order Douglas–Kroll Hamiltonian approximation (Reiher & Wolf 2004a, 2004b). The PECs and TDMs were computed for 143 single points corresponding to the internuclear distances of 0.8–10 Å (with step sizes of 0.01 Å for 0.8–1 Å, 0.02 Å for 1–2.5 Å, 0.05 Å for 2.5–3 Å, 0.1 Å for 3–6 Å, and 0.5 Å for 6–10 Å).

2.2 Radiative association cross-sections

The quantum mechanical cross-sections for the radiative association process can be expressed as

$$\sigma_{\Lambda'\rightarrow\Lambda''} = \sum_{J';\upsilon'',J''} \frac{1}{4\pi\varepsilon_0}\frac{64}{3}\frac{\pi^5}{k^2} p_{\Lambda'} \left(\frac{\nu}{c}\right)^3 S_{\Lambda',J'\rightarrow\Lambda'',J''} \times \left|M_{\Lambda',E,J';\Lambda'',\upsilon'',J''}\right|^2, \quad (2)$$

where single-primed quantities describe the initial electronic state while the double-primed ones describe the final electronic state, Λ denotes the absolute value of the projection of the electronic orbital angular momentum on the internuclear axis, ε_0 is the vacuum permittivity, $k^2 = 2\mu E/\hbar^2$, $\hbar$ is the reduced Planck constant, ν denotes the frequency of the emitted photon, c denotes the speed of light in vacuum, and $S_{\Lambda',\ J'\rightarrow\Lambda'',\ J''}$ is the Hönl–London factor (Hansson & Watson 2005; Watson 2008). The $p_{\Lambda'}$ is the statistical weight or the probability of collision in the initial electronic state Λ', given by

$$p_{\Lambda'} = \frac{(2S+1)\left(2-\delta_{0,\Lambda}\right)}{(2L_N+1)(2S_N+1)(2L_{N^+}+1)(2S_{N^+}+1)}, \quad (3)$$

where δ is the Kronecker delta; S is the spin quantum number of the electronic state Λ'; L_N, S_N, L_{N^+}, and S_{N^+} are the electronic orbital angular momentum number and spin quantum number of the atomic N and the ionic N^+, respectively. Hence, the values of $p_{\Lambda'}$ are 2/36 for $\Lambda' = X^2\Sigma_g^+$ and $B^2\Sigma_u^+$ states; 4/36 for $\Lambda' = A^2\Pi_u$, $D^2\Pi_g$, $1^4\Sigma_g^+$, and $a^4\Sigma_u^+$ states; 8/36 for $\Lambda' = f^4\Pi_u$ and $b^4\Pi_g$ states; 6/36 for $1^6\Sigma_g^+$ and $1^6\Sigma_u^+$ states; and 12/36 for $\Lambda' = 1^6\Pi_u$ and $1^6\Pi_g$ states. $M_{\Lambda',\ E,\ J';\ \Lambda'',\ \upsilon'',\ J''}$ are the radial matrix elements, given by the following integral

$$M_{\Lambda',E,J';\Lambda'',\upsilon'',J''} = \int_0^\infty \chi_{E,J'}^{\Lambda'}(R)\, D_{\Lambda'\Lambda''}(R)\, \psi_{\upsilon'',J''}^{\Lambda''}(R)\, \mathrm{d}R, \quad (4)$$

where $\chi_{E,J'}^{\Lambda'}(R)$ is the radial wavefunction of an initial continuum state, $\psi_{\upsilon'',J''}^{\Lambda''}(R)$ is the radial wavefunction of a ro-vibrational bound state, and $D_{\Lambda'\Lambda''}(R)$ is the electric TDM between Λ' and Λ''. The bound and continuum wavefunctions are obtained by the renormalized Numerov method (Johnson 1977, 1978).

2.3 Rate coefficients

The total thermal rate coefficients for the formation of a bound molecule can be expressed by

$$\alpha_{tot}(T) = \sum_{\Lambda'\rightarrow\Lambda''} \alpha_{\Lambda'\rightarrow\Lambda''}(T), \quad (5)$$

where $\alpha_{\Lambda'\rightarrow\Lambda''}(T)$ denotes the thermal rate coefficient for a two-state electronic transition process, $\alpha_{\Lambda'\rightarrow\Lambda''}$, which can be expressed as a function of temperature T

$$\alpha_{\Lambda'\rightarrow\Lambda''}(T) = \left(\frac{8}{\mu\pi}\right)^{1/2}\left(\frac{1}{k_B T}\right)^{3/2}\int_0^\infty E\sigma_{\Lambda'\rightarrow\Lambda''}(E)\exp\left(-\frac{E}{k_B T}\right)\mathrm{d}E, \quad (6)$$

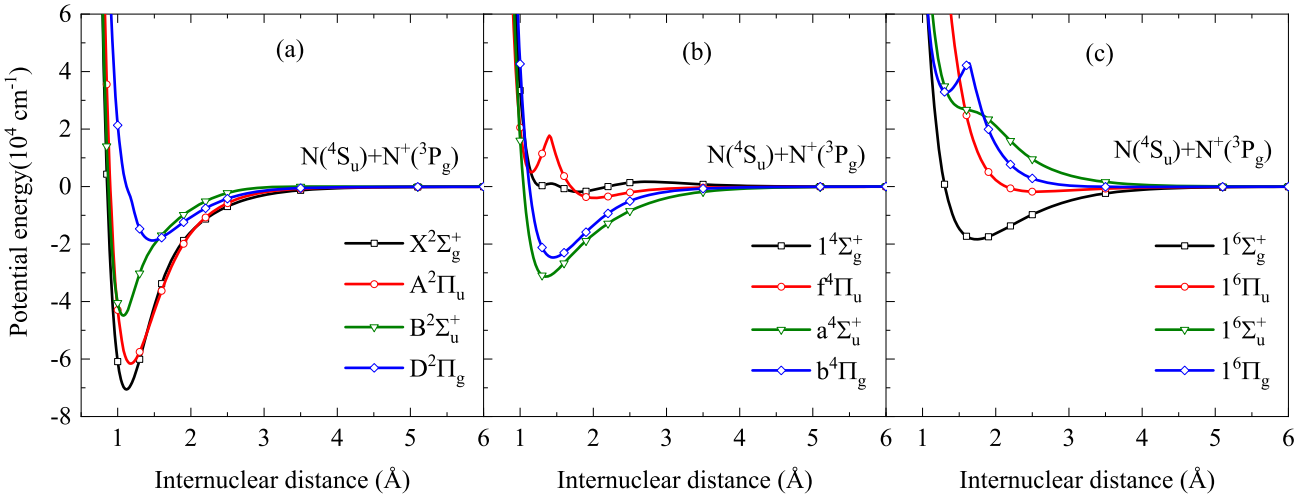

Figure 1. Potential energy curves of the (a) doublet, (b) quartet, and (c) sextet electronic states for N_2^+ calculated at the icMRCI/aug-cc-pCV5Z-DK level of theory.

where μ is the reduced mass, k_B is the Boltzmann constant, E is the collision energy, and $\sigma_{\Lambda'\rightarrow\Lambda''}$ is the cross-section for the $\Lambda'\rightarrow\Lambda''$ transition.

3 RESULTS

3.1 PECs and TDMs

The PECs of twelve electronic states for N_2^+ were calculated at the icMRCI+Q/aug-cc-pCV5Z-DK level of theory and displayed in Fig. 1 as a function of the internuclear distance R. The $1^4\Sigma_g^+$ state has two shallow potential wells. The $f^4\Pi_u$ state also has two potential wells in which one is above the dissociation limit. The $1^6\Pi_g$ state has a small potential well above the dissociation limit. The $1^6\Sigma_u^+$ state is repulsive but decreases very slowly at the internuclear distances $R = 1.4$–1.9 Å. Other electronic states are bound. To check the accuracy of the PECs, we determined the spectroscopic constants. First, the PECs were introduced into the radial Schrödinger equation to obtain the ro-vibrational energy levels. Then, the ro-vibrational energy levels were used to fit the spectroscopic parameters, which were presented in Table 1, along with available experimental values and the recent MRCI + Q/CV + DK + 56 calculations from Liu et al. (2014), who presented a comprehensive tabulation of the results calculated by earlier researchers. Compared with the recent calculations from Liu et al. (2014), our spectroscopic parameters agree well with them except the $1^6\Pi_g$ state. The calculated B_e of the $1^6\Pi_g$ state is 1.3725 cm^{-1}, while Liu et al. (2014) predicted B_e to be 0.3072 cm^{-1}. Comparisons of spectroscopic constants with available experiments are discussed below.

The $X^2\Sigma_g^+$ state is deeply bound with an equilibrium internuclear distance R_e of 1.1169 Å and a dissociation energy D_e of 8.8034 eV. The deviation of R_e relative to the experimental one (Huber & Herzberg 1979) is only 0.0005 Å. The experimental values of D_e are 8.8483 eV (Huber & Herzberg 1979) and 8.7076 ± 0.0010 eV (Tang et al. 2005). Our calculated D_e is between these two experimental results. The first excited $A^2\Pi_u$ state is computed to lie at 9116.35 cm^{-1} relative to the minimum of the ground state. Our calculated T_e is about 51 cm^{-1} smaller than the observed one of 9167.47 cm^{-1} (Scholl, Holt & Rosner 1998). The calculated R_e is 1.1744 Å, which is 0.0005 Å smaller than the experimentally determined one (Huber & Herzberg 1979). The calculated D_e value is 7.6728 eV, which is 0.0389 eV smaller than the experimental one (Huber & Herzberg 1979). For the $B^2\Sigma_u^+$ state, the calculated T_e is about 73 cm^{-1} larger than the experimentally ones of 25 461.46 cm^{-1} (Huber & Herzberg 1979) and 25 461.064 cm^{-1} (Scholl et al. 1998). The estimated dissociation energy is 5.6424 eV, which is 0.0491 eV smaller than the experimental value (Huber & Herzberg 1979). For the $D^2\Pi_g$ state, the calculated R_e is 1.4730 Å, which is 0.002 Å larger than the experimental one (Huber & Herzberg 1979). The T_e is 52 183.39 cm^{-1}, about 135 cm^{-1} smaller than the experimental value (Huber & Herzberg 1979). The calculated D_e value is 0.0307 eV smaller than the experimental one (Huber & Herzberg 1979). Overall, the deviation of the R_e value between the calculated one and the experimental values is smaller than 0.002 Å for the $X^2\Sigma_g^+$, $A^2\Pi_u$, $B^2\Sigma_u^+$, and $D^2\Pi_g$ states. For T_e and D_e, the deviations are smaller than 150 cm^{-1} and 0.05 eV, respectively. The vibrational and rotational spectroscopic constants ω_e, $\omega_e x_e$, B_e, and α_e (shown in Table 1) are in good agreement with the experimental results.

For $R > 10$ Å, the PECs were fitted by the following function

$$V(R) = \frac{C_3}{R^3} - \frac{\alpha_d(\mathrm{N})}{2R^4}, \tag{7}$$

where C_3/R^3 is the electric charge–atomic–quadrupole interaction potential energy (Gentry & Giese 1977) and α_d(N) is the static electric dipole polarizability of nitrogen (Molof et al. 1974; Zeiss & Meath 1977; Buchachenko 2011; Schwerdtfeger & Nagle 2019). We used the $C_3 = 0$ from Gentry & Giese (1977) and $\alpha_d(\mathrm{N}) = 7.4$ recommended by Schwerdtfeger & Nagle (2019) here. For $R < 0.8$ Å, the PECs were extrapolated by the following function

$$V(R) = A\exp(-BR) + C, \tag{8}$$

where A, B, and C are fitting parameters.

The TDMs for twelve dipole-allowed transitions of N_2^+ are calculated by the icMRCI/aug-cc-pCV5Z-DK method and presented in Fig. 2. To verify our TDM values, we compared our results with available ones in previous papers. Fig. 3(a) shows good agreement of the TDM values for the $A^2\Pi_u$-$X^2\Sigma_g^+$ system with those computed by Langhoff & Bauschlicher (1988). Similarly, Fig. 3(b) shows excellent agreement of the TDM values of four quartet transition systems with the calculations from Hochlaf, Chambaud & Rosmus (1997) except for the $1^4\Sigma_g^+$-$a^4\Sigma_u^+$ system. Although our TDM values of the $1^4\Sigma_g^+$-

Table 1. Spectroscopic constants for the electronic states of N_2^+ by the present icMRCI + Q/aug-cc-pCV5Z-DK calculation along with other theoretical and experimental results.

State	Source	R_e (Å)	T_e (cm^{-1})	ω_e (cm^{-1})	$\omega_e x_e$(cm^{-1})	B_e (cm^{-1})	$10^2\alpha_e$ (cm^{-1})	D_e (eV)
$X^2\Sigma_g^+$	This work	1.1169	0.00	2206.46	16.73	1.9300	1.872	8.8034
	Expt.[a]	1.1164	0.00	2207.00	16.10	1.93 176	1.881	8.8483
	Expt.[b]	–	0.00	2207.252	16.256	1.93 173	1.874	–
	Expt.[c]	–	–	–	–	–	–	8.7076 ± 0.0010
	Calc.[d]	1.1167	0.00	2207.58	16.625	1.9305	1.811	8.8796
$A^2\Pi_u$	This work	1.1744	9116.35	1901.26	15.11	1.7443	1.948	7.6728
	Expt.[a]	1.1749	–	1903.70	15.02	1.7444	1.883	7.7117
	Expt.[b]	–	9167.47	1903.70	15.111	1.7445	1.87	–
	Calc.[d]	1.1750	9088.23	1904.59	15.033	1.7444	1.8640	7.7393
$B^2\Sigma_u^+$	This work	1.0751	25 534.39	2417.77	26.49	2.0825	2.12	5.6424
	Expt.[a]	1.0742	25 461.46	2419.84	23.189	2.07 456	2.4	5.6915
	Expt.[b]	–	25 461.064	2421.14	24.07	2.08 533	2.12	–
	Calc.[d]	1.0748	25 551.02	2419.61	21.535	2.0840	2.1676	5.6927
$a^4\Sigma_u^+$	This work	1.3498	39 380.57	1165.10	15.45	1.3219	2.37	3.9248
	Calc.[d]	1.3482	39 595.86	1182.13	16.906	1.3247	2.2995	3.9725
$b^4\Pi_g$	This work	1.4499	46 161.57	1008.39	11.36	1.1453	1.73	3.0823
	Calc.[d]	1.4483	46 408.35	1008.75	11.416	1.1477	1.7556	3.1135
$D^2\Pi_g$	This work	1.4730	52 183.89	906.59	12.48	1.1097	2.01	2.3310
	Expt.[a]	1.471	52 318.2	907.71	11.91	1.113	2.0	2.3617
	Calc.[d]	1.4705	52 376.08	909.60	11.91	1.1051	1.8644	2.3545
$1^6\Sigma_g^+$	This work	1.7339	52 402.77	651.82	5.877	0.8011	1.08	2.3030
	Calc.[d]	1.7338	52 736.46	652.64	6.2123	0.8009	1.0908	2.3221
$1^6\Pi_u$	This work	2.5474	69 143.88	220.95	6.72	0.3710	1.18	0.2283
	Calc.[d]	2.5453	69 517.71	222.47	6.5617	0.3716	1.1818	0.2407
$f^4\Pi_u(1^{st}$ well)	This work	1.1514	75 556.34	2092.45	20.76	1.8157	1.74	2.5427
	Calc.[d]	1.1515	75 726.43	2099.73	22.425	1.8201	2.6427	1.6276
$f^4\Pi_u(2^{nd}$ well)	This work	2.0128	66 967.13	449.83	10.98	0.5941	1.24	0.4959
	Calc.[d]	2.0103	67 382.44	452.15	8.7608	0.5957	1.2450	0.5131
$1^6\Pi_g$	This work	1.3244	103 434.99	1504.20	13.14	1.3725	1.42	1.2817
	Calc.[d]	1.3236	103 803.38	1474.84	99.887	0.3072	373.49	1.1951

Notes. [a]Huber & Herzberg (1979); [b]Scholl et al. (1998); [c]Tang et al. (2005); [d]Liu et al. (2014).

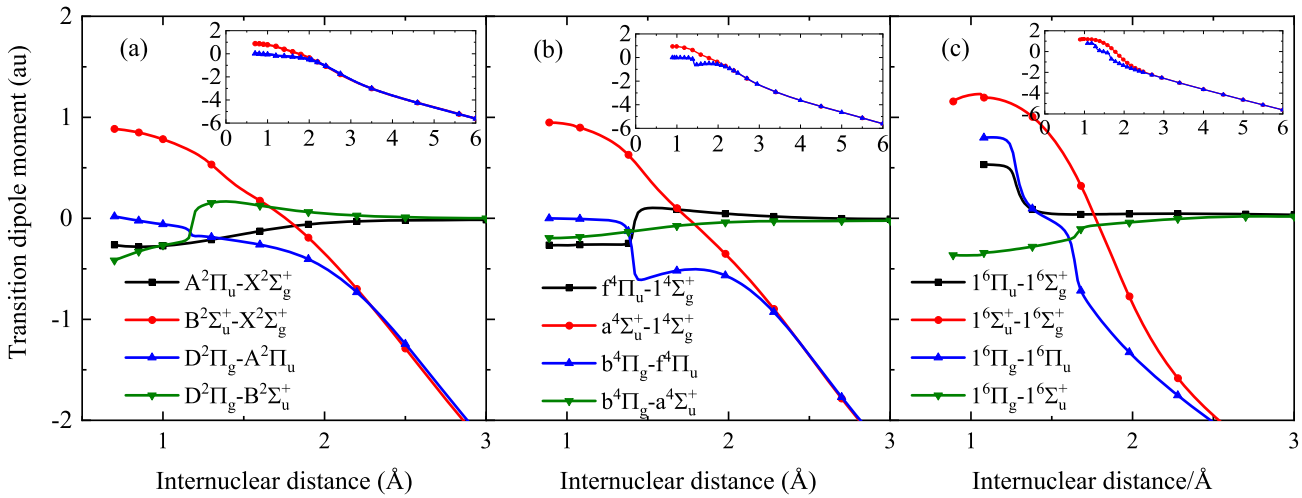

Figure 2. Transition dipole moments for the (a) doublet, (b) quartet, and (c) sextet transitions of N_2^+ as a function of the internuclear distance *R*.

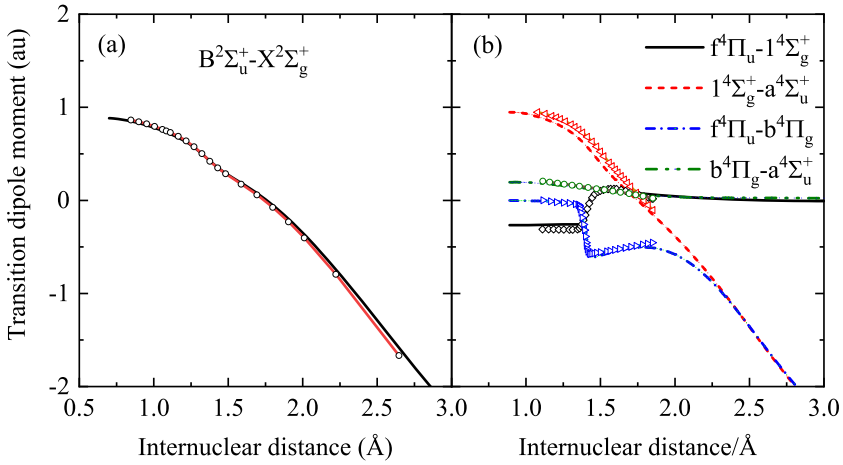

Figure 3. Transition dipole moments of (a) the $B^2\Sigma_u^+-X^2\Sigma_g^+$ system and (b) the $f^4\Pi_u$-$1^4\Sigma_g^+$, $a^4\Sigma_u^+$-$1^4\Sigma_g^+$, $b^4\Pi_g$- $f^4\Pi_u$, and $b^4\Pi_g$-$a^4\Sigma_u^+$ systems of N_2^+: The lines are from this work; the symbol in (a) represents the computed values from Langhoff & Bauschlicher (1988); the symbols in (b) represent the computed values from Hochlaf et al. (1997).

$a^4\Sigma_u^+$ system exhibit a little smaller than those computed by Hochlaf et al. (1997). However, the trend of the two sets of the TDM values along R is similar. The slight deviation may result from the different levels of theory.

As shown in the insets of Fig. 2, the TDM values for the $\Sigma_u^+-\Sigma_g^+$ and Π_g-Π_u systems approach $-(R-0.385)$ au for $R \geq 4$ Å. That is, the TDM value varies linearly with the internuclear distance R ($R \geq 4$ Å), which can be expressed as

$$D\,(\mathrm{TDMvalue}) \approx -(R-0.385)\ . \tag{9}$$

For example, the TDM value is close to $-(4-0.385) = -3.615$ au when $R = 4$ Å. Also, the TDM value is close to $-(5-0.385) = -4.615$ au when $R = 5$ Å. Such situation is similar to the $A^2\Pi_u$-$X^2\Pi_g$ TDM of O_2^+(Wetmore, Fox & Dalgarno 1984), also similar to the TDMs of the $B^4\Sigma_u^- - X^4\Sigma_g^-$, $f^2\Pi_g - a^2\Pi_u$, and $2^2\Pi_g - 2^2\Pi_u$ transitions for C_2^+(Babb et al. 2019a). For other transition systems of N_2^+, the TDM values approach 0 for large R. Therefore, the TDMs were fitted to the form $1/R^4$ for $R > 10$ Å except for the $\Sigma_u^+-\Sigma_g^+$ and Π_g-Π_u systems, which were fitted to $-(R-0.385)$ at large internuclear distances.

3.2 Radiative association cross-sections

In the considered twelve electronic states mentioned above, there exist twelve dipole-allowed transitions. The transitions between the $1^4\Sigma_g^+$ and $f^4\Pi_u$ states, and the $1^6\Sigma_u^+$ and $1^6\Pi_g$ states are not considered here because these states have shallow potential wells, which are expected to contribute little to the radiative association in the collision of $N(^4S_u)$ and $N^+(^3P_g)$. The remaining ten transitions, including $A^2\Pi_u \rightarrow X^2\Sigma_g^+$, $B^2\Sigma_u^+ \rightarrow X^2\Sigma_g^+$, $D^2\Pi_g \rightarrow A^2\Pi_u$, $D^2\Pi_g \rightarrow B^2\Sigma_u^+$, $1^4\Sigma_g^+ \rightarrow a^4\Sigma_u^+$, $f^4\Pi_u \rightarrow b^4\Pi_g$, $b^4\Pi_g \rightarrow a^4\Sigma_u^+$, $1^6\Pi_u \rightarrow 1^6\Sigma_g^+$, $1^6\Sigma_u^+ \rightarrow 1^6\Sigma_g^+$, and $1^6\Pi_g \rightarrow 1^6\Pi_u$, are taken into account to compute the cross-sections of N_2^+. The results are plotted in Fig. 4. Numerous shape resonances are visible. For the $1^4\Sigma_g^+ \rightarrow a^4\Sigma_u^+$ transition process, the resonance tunnelling feature is visible, which results from the fact that the $1^4\Sigma_g^+$ state exhibits a potential barrier (local maximum) in the entrance channel. The local maximum of the PEC is 0.21 eV at $R = 2.75$ Å for the $1^4\Sigma_g^+$ state. The corresponding cross-section decreases sharply below 0.21 eV.

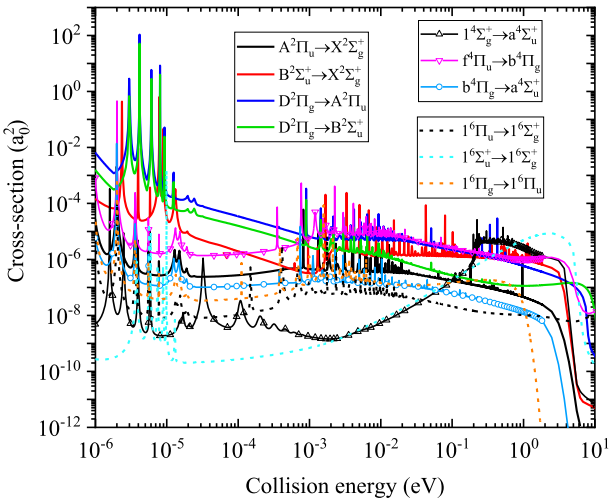

Figure 4. Radiative association cross-sections (in units of a_0^2) as a function of the collision energy E (eV) for the collision of $N(^4S_u)$ and $N^+(^3P_g)$: The doublet transitions are given in solid lines, the quartet transitions are given in solid lines with symbols, and the sextet transitions are given in dashed lines.

As shown in Fig. 4, the $D^2\Pi_g \rightarrow A^2\Pi_u$ cross-sections are the largest ones for the calculated energies E smaller than about 1×10^{-3} eV, followed by the $D^2\Pi_g \rightarrow B^2\Sigma_u^+$ and $B^2\Sigma_u^+ \rightarrow X^2\Sigma_g^+$ systems. For energies E larger than 1×10^{-3} eV but lower than 0.2 eV, the $f^4\Pi_u \rightarrow b^4\Pi_g$ transition dominates most, followed by the $D^2\Pi_g \rightarrow A^2\Pi_u$ and $B^2\Sigma_u^+ \rightarrow X^2\Sigma_g^+$ systems. Subsequently, the $1^4\Sigma_g^+ \rightarrow a^4\Sigma_u^+$ transition dominates over the energy range of about 0.2–0.8 eV. Above 0.8 eV, the $1^6\Sigma_u^+ \rightarrow 1^6\Sigma_g^+$ transition is dominant. Other transition processes are relatively weaker and will not contribute significantly to the total cross-sections. The relatively large values of the $f^4\Pi_u \rightarrow b^4\Pi_g$, $D^2\Pi_g \rightarrow A^2\Pi_u$, and $B^2\Sigma_u^+ \rightarrow X^2\Sigma_g^+$ transitions over a large energy range can be explained as follows. The TDMs for these three transition processes are generally large, in particular at the internuclear distances corresponding to the potential wells of the related electronic states (as seen in Figs 1 and 2). Moreover, the potential wells of the $X^2\Sigma_g^+$, $A^2\Pi_u$, and $b^4\Pi_g$ states

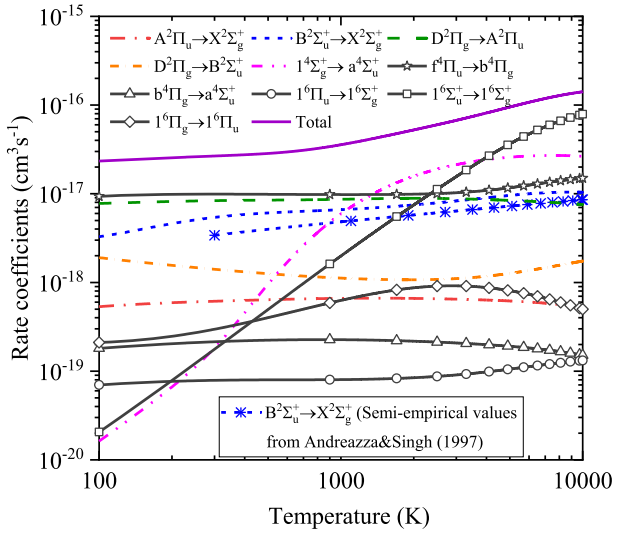

Figure 5. The total rate coefficient and rate coefficients (in units of $cm^3\ s^{-1}$) of the ten studied transitions for the formation of N_2^+ by radiative association process (1). The rate coefficient for the $B^2\Sigma_u^+ \rightarrow X^2\Sigma_g^+$ transition computed by Andreazza & Singh (1997) is also presented for comparison.

are relatively deep and can support many ro-vibrational bound levels to which radiative association transitions can occur.

3.3 Rate coefficients

The rate coefficients were calculated by integrating the cross-sections over a Maxwellian velocity distribution [equation (6)] in the range of 100–10 000 K. The results for ten transition processes mentioned above and the total rate coefficients are shown in Fig. 5. The contributions of the $f^4\Pi_u \rightarrow b^4\Pi_g$, $D^2\Pi_g \rightarrow A^2\Pi_u$, and $B^2\Sigma_u^+ \rightarrow X^2\Sigma_g^+$ transitions to the total rate coefficients are relatively large, especially for the temperatures lower than about 1400 K. For temperatures larger than 1400 K, the $1^4\Sigma_g^+ \rightarrow a^4\Sigma_u^+$ transition contributes most until about 3800 K. Above 3800 K, the $1^6\Sigma_u^+ \rightarrow 1^6\Sigma_g^+$ transition makes the largest contribution. Although the $1^6\Sigma_u^+$ state is repulsive, the $1^6\Sigma_g^+$ state has a potential well of about 18 575 cm^{-1} which can support 53 vibrational levels. Also, the TDM values for the $1^6\Sigma_u^+ \rightarrow 1^6\Sigma_g^+$ transition are large enough along the internuclear distance. These may be the reason that the $1^6\Sigma_u^+ \rightarrow 1^6\Sigma_g^+$ transition dominates above 3800 K. For the $A^2\Pi_u \rightarrow X^2\Sigma_g^+$, $b^4\Pi_g \rightarrow a^4\Sigma_u^+$, $1^6\Pi_u \rightarrow 1^6\Sigma_g^+$, and $1^6\Pi_g \rightarrow 1^6\Pi_u$ transitions, the rate coefficients are at least one-order magnitude lower than those for the $f^4\Pi_u \rightarrow b^4\Pi_g$, $D^2\Pi_g \rightarrow A^2\Pi_u$, and $B^2\Sigma_u^+ \rightarrow X^2\Sigma_g^+$ transitions except for $D^2\Pi_g \rightarrow B^2\Sigma_u^+$ transition. It should be noted that the rate coefficients for the $1^4\Sigma_g^+ \rightarrow a^4\Sigma_u^+$ and $1^6\Sigma_u^+ \rightarrow 1^6\Sigma_g^+$ transitions increase monotonically as the temperature increases because the $1^6\Sigma_u^+$ state is repulsive and the $1^4\Sigma_g^+$ state has two very shallow potential wells. Such similar behaviours can be found from previous publications (Gustafsson, Monge-Palacios & Nyman 2014; Bai, Qin & Liu 2021).

Andreazza & Singh (1997) investigated the radiative association of $N(^4S_u)$ and $N^+(^3P_g)$ by considering the $A^2\Pi_u \rightarrow X^2\Sigma_g^+$ and $B^2\Sigma_u^+ \rightarrow X^2\Sigma_g^+$ transitions. They computed the cross-sections by the semi-empirical method but not presented them in their work. They estimated the contribution of the $A^2\Pi_u \rightarrow X^2\Sigma_g^+$ transition to the rate coefficients of N_2^+ to be small. Our determined values of the rate coefficients for the $A^2\Pi_u \rightarrow X^2\Sigma_g^+$ transition by the quantum mechanical theory also exhibit an insignificant contribution. The rate coefficients for the $B^2\Sigma_u^+ \rightarrow X^2\Sigma_g^+$ transition estimated by Andreazza & Singh (1997) are also presented in Fig. 5 and increase slowly over the temperature range from 300 to 14 700 K, varying from about 3.4×10^{-18} to 9.42×10^{-18} $cm^3\ s^{-1}$. The rate coefficients for the $B^2\Sigma_u^+ \rightarrow X^2\Sigma_g^+$ transition calculated in this work are slightly larger than those obtained by Andreazza & Singh (1997). The deviation decreases as the temperature increases.

In the present calculations, the dominant transition processes for the formation of N_2^+ include not only the $B^2\Sigma_u^+ \rightarrow X^2\Sigma_g^+$ transition, but also the $f^4\Pi_u \rightarrow b^4\Pi_g$, $D^2\Pi_g \rightarrow A^2\Pi_u$, $1^4\Sigma_g^+ \rightarrow a^4\Sigma_u^+$, and $1^6\Sigma_u^+ \rightarrow 1^6\Sigma_g^+$ transitions, depending on different temperature ranges. Hence, the total rate coefficients estimated here are larger than the values estimated by Andreazza & Singh (1997). Moreover, the rate coefficients for temperatures from 100 to 300 K are also provided here. The fit function using the rate coefficients from Andreazza & Singh (1997) has been chosen as applicable for $300 < T < 14\,700$ K in the UMIST RATE2012[1], the UMIST data base for astrochemistry. The improved rate coefficients for the formation of N_2^+ by radiative association are presented in this work and can be fitted to better than 6 per cent by the following function

$$\alpha(T) = a + bT + cT^2 + dT^3, \quad 100 \leq T \leq 10\,000\ \mathrm{K}, \tag{10}$$

where a, b, c, and d are fitting parameters, $a = 2.08\,527 \times 10^{-17}$, $b = 1.5707 \times 10^{-20}$, $c = 2.95\,637 \times 10^{-26}$, and $d = -3.99\,714 \times 10^{-29}$.

4 CONCLUSION

In this work, we have computed the cross-sections and rate coefficients for the formation of N_2^+ by radiative association in the collision of $N(^4S_u)$ and $N^+(^3P_g)$. Ten transition processes contributing to the reaction (1) have been considered based on a new set of PECs and TDMs calculated at the icMRCI+Q/aug-cc-pCV5Z-DK level of theory. The results show that the dominant transition processes are different for different temperature ranges. The contributions of the $f^4\Pi_u \rightarrow b^4\Pi_g$, $D^2\Pi_g \rightarrow A^2\Pi_u$, and $B^2\Sigma_u^+ \rightarrow X^2\Sigma_g^+$ transitions to the total rate coefficients are relatively large, especially for the temperatures lower than about 1400 K. For temperatures larger than about 1400 K, the contributions of the $1^4\Sigma_g^+ \rightarrow a^4\Sigma_u^+$ and $1^6\Sigma_u^+ \rightarrow 1^6\Sigma_g^+$ transitions are relatively significant. The computed cross-sections and rate coefficients are likely suitable for applicability in the chemistry of nitrogen-rich atmospheres (Dutuit et al. 2013) and interstellar clouds subjected to X-rays (Sun et al. 1996; Andreazza & Singh 1997).

ACKNOWLEDGEMENTS

This work is sponsored by the National Natural Science Foundation of China under grant no. 51421063. This work is also supported by the Postdoctoral Applied Research Project of Qingdao. The scientific calculations in this paper have been done on the HPC Cloud Platform of Shandong University.

CONFLICT OF INTEREST

The authors declare that they have no known competing financial interests or personal relationships that could have appeared to influence the work reported in this paper.

[1] http://udfa.ajmarkwick.net/

DATA AVAILABILITY

Full data are available. The cross-sections and rate coefficients can be obtained online at https://dr-zhi-qin.github.io/personal/Database.html. The rate coefficients for the $A^2\Pi_u \rightarrow X^2\Sigma_g^+$, $B^2\Sigma_u^+ \rightarrow X^2\Sigma_g^+$, $D^2\Pi_g \rightarrow A^2\Pi_u$, $D^2\Pi_g \rightarrow B^2\Sigma_u^+$, $1^4\Sigma_g^+ \rightarrow a^4\Sigma_u^+$, $f^4\Pi_u \rightarrow b^4\Pi_g$, $b^4\Pi_g \rightarrow a^4\Sigma_u^+$, $1^6\Pi_u \rightarrow 1^6\Sigma_g^+$, $1^6\Sigma_u^+ \rightarrow 1^6\Sigma_g^+$, and $1^6\Pi_g \rightarrow 1^6\Pi_u$ transitions, together with the total rate coefficients of N_2^+ (corresponding to Fig. 5) are provided in the supplemental material.

REFERENCES

Andreazza C. M., Marinho E. P., 2007, MNRAS, 380, 365
Andreazza C. M., Singh P. D., 1997, MNRAS, 287, 287
Andreazza C. M., Vichietti R. M., Marinho E. P., 2009, MNRAS, 400, 1892
Andreazza C. M., de Almeida A. A., Vichietti R. M., Ceccatto D. T., 2012, MNRAS, 427, 833
Andreazza C. M., de Almeida A. A., Borin A. C., 2016, MNRAS, 457, 3096
Andreazza C. M., de Almeida A. A., Vichietti R. M., 2018, MNRAS, 477, 548
Babb J. F., Smyth R. T., McLaughlin B. M., 2019a, ApJ, 876, 38
Babb J. F., Smyth R. T., McLaughlin B. M., 2019b, ApJ, 884, 155
Bai T., Qin Z., Liu L., 2021, MNRAS, 500, 2496
Barinovs Ğ., van Hemert M. C., 2006, ApJ, 636, 923
Broadfoot A. L., Hunten D. M., 1966, PSS, 14, 1303
Buchachenko A. A., 2011, PRSA, 467, 1310
Cairnie M., Forrey R. C., Babb J. F., Stancil P. C., McLaughlin B. M., 2017, MNRAS, 471, 2481
Chamberlain J. W., 1961, Physics of the Aurora and Airglow. Academic press, UK
Cravens T. E. et al., 2006, Geophys. Res. Lett., 33, L07105
de Almeida A. A., Andreazza C. M., Borin A. C., 2020, Theor. Chem. Acc., 139, 1
Dutuit O. et al., 2013, ApJS, 204, 20
Erkaev N. V., Scherf M., Thaller S. E., Lammer H., Mezentsev A. V., Ivanov V. A., Mandt K. E., 2021, MNRAS, 500, 2020
Falcinelli S., Pirani F., Alagia M., Schio L., Richter R., Stranges S., Balucani N., Vecchiocattivi F., 2016, The 1st International Electronic Conference on Atmospheric Sciences (ECAS 2016). p. 16
Fehsenfeld F. C., Dunkin D. B., Ferguson E. E., 1970, PSS, 18, 1267
Feldman P. D., 1973, J. Geophys. Res., 78, 2010
Forrey R. C., Babb J. F., Courtney E. D. S., McArdle R. T., Stancil P. C., 2020, ApJ, 898, 86
Forrey R. C., Babb J. F., Stancil P. C., McLaughlin B. M., 2018, MNRAS, 479, 4727
Gentry W. R., Giese C. F., 1977, J. Chem. Phys., 67, 2355
Gianturco F. A., Giorgi P. G., 1997, ApJ, 479, 560
Gustafsson M., Forrey R. C., 2019, J. Chem. Phys., 150, 224301
Gustafsson M., Monge-Palacios M., Nyman G., 2014, J. Chem. Phys., 140, 184301
Hansson A., Watson J. K. G., 2005, J. Mol. Spectrosc., 233, 169
Herzberg G., 1950, Molecular Spectra and Molecular Structure, Vol. 1: Spectra of Diatomic Molecules. Van Nostrand Reinhold, New York
Herzberg G., 1971, Q. Rev. Chem. Soc., 25, 201
Hochlaf M., Chambaud G., Rosmus P., 1997, J. Phys. B, 30, 4509
Huber K.-P., Herzberg G., 1979, Molecular Spectra and Molecular Structure: IV. Constants of Diatomic Molecules. Springer-Verlag, Berlin
Johnson B. R., 1977, J. Chem. Phys., 67, 4086
Johnson B. R., 1978, J. Chem. Phys., 69, 4678
Jones A. V., 1971, Space Sci. Rev., 11, 776
Knowles P. J., Werner H.-J., 1985, Chem. Phys. Lett., 115, 259
Knowles P. J., Werner H.-J., 1988, Chem. Phys. Lett., 145, 514
Knowles P. J., Werner H. -J., 1992, Theor. Chim. Acta, 84, 95
Langhoff S. R., Bauschlicher C. W., Jr, 1988, J. Chem. Phys., 88, 329
Liu H., Shi D., Wang S., Sun J., Zhu Z., 2014, J. Quant. Spectrosc. Radiat. Transfer, 147, 207
Lofthus A., Krupenie P. H., 1977, J. Phys. Chem. Ref. Data, 6, 113
McCormack B. M., 1971, The Radiating Atmosphere. Reidel, Holland
McElroy D., Walsh C., Markwick A. J., Cordiner M. A., Smith K., Millar T. J., 2013, A&A, 550, A36
Molof R. W., Schwartz H. L., Miller T. M., Bederson B., 1974, Phys. Rev. A, 10, 1131
Nyman G., Gustafsson M., Antipov S. V., 2015, Int. Rev. Phys. Chem., 34, 385
Paschmann G., Haaland S., Treumann R., 2012, Auroral Plasma Physics. Springer Sci. Bus. Media, Dordrecht
Raghuram S., Bhardwaj A., Hutsemékers D., Opitom C., Manfroid J., Jehin E., 2021, MNRAS, 501, 4035
Reiher M., Wolf A., 2004a, J. Chem. Phys., 121, 2037
Reiher M., Wolf A., 2004b, J. Chem. Phys., 121, 10945
Scherf M., Lammer H., Erkaev N. V., Mandt K. E., Thaller S. E., Marty B., 2020, Space Sci. Rev., 216, 1
Scholl T. J., Holt R. A., Rosner S. D., 1998, J. Mol. Spectrosc., 192, 424
Schwerdtfeger P., Nagle J. K., 2019, Mol. Phys., 117, 1200
Shamasundar K. R., Knizia G., Werner H.-J., 2011, J. Chem. Phys., 135, 054101
Sharp W. E., 1974, J. Geophys. Res., 79, 1569
Singh P. D., Sanzovo G. C., Borin A. C., Ornellas F. R., 1999, MNRAS, 303, 235
Slipher V. M., 1933, MNRAS, 93, 657
Stancil P. C., Dalgarno A., 1997, ApJ, 479, 543
Stancil P. C., Kirby K., Gu J.-P., Hirsch G., Buenker R. J., Sannigrahi A. B., 2000, A&AS, 142, 107
Sun Y., Sadeghpour H. R., Kirby K., Dalgarno A., Lafyatis G. P., 1996, Int. Rev. Phys. Chem., 15, 53
Swings P., 1943, MNRAS, 103, 86
Tang X., Hou Y., Ng C. Y., Ruscic B., 2005, J. Chem. Phys., 123, 074330
Venkataramani K., Ganesh S., 2018, EPSC Abstracts Vol. 12, Results from two unusual comets C/2016 R2 (Pan-STARRS) and C/2015 V2 (Johnson). European Planetary Science Congress, Berlin, Germany, EPSC2018–1220
Wallace L., McElroy M. B., 1966, Planet Space Sci., 14, 677
Watson J. K., 2008, J. Mol. Spectrosc., 252, 5
Werner H.-J. et al., 2020, J. Chem. Phys., 152 144107
Werner H.-J., Knowles P. J., 1985, J. Chem. Phys., 82, 5053
Werner H.-J., Knowles P. J., 1988, J. Chem. Phys., 89, 5803
Werner H.-J., Knowles P. J., Knizia G., Manby F. R., MOLPRO, 2015, a package of ab initio programs, available at: http://www.molpro.net
Wetmore R. W., Fox J. L., Dalgarno A., 1984, Planet Space Sci., 32, 1111
Zámečníková M., Gustafsson M., Nyman G., Soldán P., 2020, MNRAS, 492, 3794
Zámečníková M., Soldán P., Gustafsson M., Nyman G., 2019, MNRAS, 489, 2954
Zeiss G. D., Meath W. J., 1977, Mol. Phys., 33, 1155
Zipf E. C., Jr, Fastie W. G., 1964, J. Geophys. Res., 69, 2357

SUPPORTING INFORMATION

Supplementary data are available at *MNRAS* online.

N2+_rate_coefficients.txt.

Please note: Oxford University Press is not responsible for the content or functionality of any supporting materials supplied by the authors. Any queries (other than missing material) should be directed to the corresponding author for the article.

This paper has been typeset from a TEX/LATEX file prepared by the author.